Time-dependent injection rates and linearized interfacial motion in multi-layer Hele-Shaw and porous media flows

Craig Gin[1] and Prabir Daripa[1]†

[1]Department of Mathematics , Texas A&M University, College Station, TX 77843

(Received xx; revised xx; accepted xx)

We study the stability of multi-layer radial flows in porous media within the Hele-Shaw model. The study is motivated by a need to design smart injection policies for chemical enhanced oil recovery. We first consider three-layer radial flows with interfaces separating fluids of constant viscosity in each layer and with positive viscosity jump at each interface in the direction of flow. We then extend the results to flows with an arbitrary number of fluid layers. Several different time-dependent injection strategies are analyzed. In particular, we investigate the conditions on the injection rate that ensure that the flow is stable. These allow for a maximal injection rate while maintaining a stable flow. Additionally, we show that in any multi-layer radial Hele-Shaw flow, if all of the interfaces are circular except for one perturbed circular interface then there exists a time-dependent injection rate such that the circular interfaces remain circular as they propagate and the disturbance on the perturbed interface decays. This result is independent of the values of all of the parameters including viscosities of fluid layers and interfacial tensions. This time-dependent configuration consisting of all but one circular interfaces is unstable to infinitesimal disturbances to one or more of these circular interfaces at the same time-dependent injection rate. Furthermore, we also find numerically that flows with more fluid layers can be stable with faster time-dependent injection rates than comparable flows with fewer fluid layers.

The motion of the interfaces within linear theory is also investigated numerically for the case of constant injection rates. Some important results, among others, are: (i) A disturbance which is initially stable can become unstable at later times; (ii) A disturbance of one interface can be transferred to the other interface(s); (iii) The disturbances on

† Email address for correspondence: daripa@math.tamu.edu

the interfaces can develop either in phase or out of phase from any arbitrary initial disturbance; and (iv) High wavenumber disturbances are more unstable at later times compared to lower wave number disturbances.

1. Introduction

There are many applications in which one fluid displaces another fluid in a porous media including oil recovery, hydrology, filtration, and fixed bed regeneration in chemical processing. In the case that the displacing fluid is less viscous than the displaced fluid, the interface between the fluids is unstable and viscous fingering ensues. In some of the aforementioned applications, a series of fluids are used to displace the resident fluid in the porous media. An example of this is chemical enhanced oil recovery (EOR) in which a sequence of complex fluids with favorable properties are injected into an oil reservoir. If the properties of these fluids and the injection procedure are chosen properly then there can be significant improvement in oil recovery over water flooding methods. It is well-known that viscous fingering limits the displacement efficiency in such processes so controlling this instability is very important for industrial applications.

Viscous fingering in porous media flows (Homsy 1987) is often studied using the Hele-Shaw model, meaning that there is a sharp interface between immiscible fluids. A linear stability analysis of viscous fingering within the Hele-Shaw model was first performed by Saffman & Taylor (1958). They studied the case in which the fluid moves linearly and orthogonal to a planar interface. We refer to this flow configuration as rectilinear flow. An appropriate model for flow near an injection or production well is radial flow. The stability of radial Hele-Shaw flows was first studied by Bataille (1968) and Wilson (1975) and was later developed further by Paterson (1981). Recently there have been many studies of the stability of Hele-Shaw flows with more complex physics in both the rectilinear and radial geometries. These include tapered Hele-Shaw cells (Al-Housseiny & Stone 2013), inertial effects (Dias & Miranda 2011), and flows of chemically reactive (He *et al.* 2012) or non-Newtonian fluids (Coussot 1999; Fontana *et al.* 2014), but almost all involve two layers of fluids separated by one interface initially.

There have been a few studies on flows with more than two fluid layers. Cardoso & Woods (1995) studied three-layer flows in both the rectilinear and radial flow geometries. For radial flows, they considered flows in which the inner interface is stable and used the linear theory to predict the number of drops formed when the interfaces meet. Beeson-

Jones & Woods (2015) studied three-layer radial flow and found the optimal value of the viscosity of the intermediate fluid in order to inject fluid at the fastest rate possible while maintaining a stable flow. Daripa and various collaborators have studied various aspects of multi-layer flows in both the rectilinear and radial geometries. In a paper by Daripa (2008*b*), three-layer rectilinear Hele-Shaw flows are studied and a formula is given for a critical value of the viscosity of the middle layer fluid that minimizes the bandwidth of unstable waves. Daripa also formulated the stability problem for rectilinear Hele-Shaw flows with an arbitrary number of fluid layers (Daripa 2008*a*). In this paper, variational techniques are used to derive upper bounds on the growth rate of instabilities. Similar results for multi-layer radial flow are given by Gin & Daripa (2015).

In chemical EOR, polymer is often used in the injected fluid in order to increase the viscosity and achieve a more favorable mobility ratio. In such processes, it can be the case that the fluid viscosity varies throughout the layer. The stability of variable viscosity rectilinear Hele-Shaw flows is studied extensively in several works by Daripa, et al. For example, Daripa (2008*a*) found upper bounds on the growth rate, Daripa & Ding (2012, 2013) studied the optimal viscous profile for both three-layer and four-layer flows, and Daripa & Gin (2016) studied the effect of dispersion on three-layer rectilinear flows with variable viscosity.

In controlling the instability of Hele-Shaw and porous media flows, one of the simplest parameters to control is the rate at which fluid is injected. There have been several studies on controlling the instability by using a time-dependent injection rate. The most dangerous wave number (and hence the number of fingers) can be made constant in time by considering an injection rate that scales with time like $t^{-1/3}$. This type of injection rate was studied numerically by Li *et al.* (2009) and the limiting shape of the interface is found to be independent of the initial conditions. Zheng *et al.* (2015) studied a class of time-dependent control strategies of which the $t^{-1/3}$ injection rate is a special case. Dias *et al.* (2012) studied the optimal injection policy when a given amount of fluid needs to be pumped in a given amount of time and found that a linearly increasing injection rate is optimal. Beeson-Jones & Woods (2015) found the maximum possible time-dependent injection rate for a stable flow analytically for two-layer flow and numerically for three-layer flow.

The previous works (Cardoso & Woods 1995; Gin & Daripa 2015; Beeson-Jones & Woods 2015) on such flows follow two different but equivalent formulations, each with its

strengths and weaknesses. One of the purposes of this paper is to clarify the connection between these two formulations in order to unite the knowledge base. Cardoso & Woods (1995) and Beeson-Jones & Woods (2015) make use of the potential function formulation of the problem. Their approach results in a system of ordinary differential equations (ODEs) and the growth rates of disturbances are the eigenvalues of the associated matrix. The strength of this approach is that the motion of the interfaces is very clear from the formulation. In the works of Daripa (2008*a*,*b*) and Gin & Daripa (2015), the growth rate occurs as the eigenvalue of a differential operator. Although the motion of the interfaces is somewhat obscured by this approach, it allows for the use of variational principles to obtain upper bounds on the growth rate. It also allows for the extension to variable viscosity flows. The present work uses a hybrid of these two methods in order to try to elucidate the connection between the two. Furthermore, we also study stabilization of potentially unstable multi-layer radial Hele-Shaw flows using time-dependent injection rates and the linearized motion of interfaces under constant as well as time-dependent injection rates.

The paper is laid out as follows. In §2, the stability problem is formulated for three-layer Hele-Shaw flows. The eigenvalues and eigenvectors of the resulting matrix are considered in §3. In §4, the formulation is then extended to flows with an arbitrary number of fluid layers. Several different time-dependent injection strategies that can be used to control the instability are described and analyzed in §5. Numerical results are given in §6 and then concluding remarks are given in §7.

2. Preliminaries

Three-layer flow is the fundamental building block for developing the mathematical apparatus for multi-layer flows. Therefore, we first consider radial Hele-Shaw flows consisting of three regions of incompressible, immiscible fluid. By averaging across the gap, we may consider two-dimensional flows in polar coordinates, $\Omega := (r, \theta) = \mathbb{R}^2$. The least viscous fluid with constant viscosity μ_i is injected into the center of the cell at injection rate Q. The most viscous fluid, with constant viscosity μ_o, is the outermost fluid. The intermediate fluid has constant viscosity μ_1 where $\mu_i < \mu_1 < \mu_o$. The fluid flow is governed by the following equations

$$\nabla \cdot \mathbf{u} = 0, \qquad \nabla\, p = -\mu\, \mathbf{u}, \qquad \text{for } r \neq 0. \tag{2.1}$$

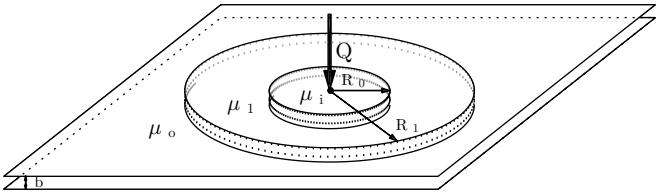

Figure 1: The basic solution for three-layer flow

The first equation $(2.1)_1$ is the continuity equation for incompressible flow, and the second equation $(2.1)_2$ is Darcy's law (Darcy 1856). We start with the fluids separated by circular interfaces with radii $R_0(0)$ and $R_1(0)$, where $R_0(t)$ and $R_1(t)$ are the positions of the interfaces at time t. This set-up is shown in Figure 1.

The equations admit a simple basic solution in which all of the fluid moves outward radially with velocity $\mathbf{u} := (u_r, u_\theta) = (Q/(2\pi r), 0)$. The interfaces remain circular and their radii are given by $R_0(t) = \sqrt{Qt/\pi + R_0(0)^2}$ and $R_1(t) = \sqrt{Qt/\pi + R_1(0)^2}$. The pressure, $p = p(r)$, may be obtained by integrating equation $(2.1)_2$.

We perturb the basic solution (u_r, u_θ, p) by $(\tilde{u_r}, \tilde{u_\theta}, \tilde{p})$. Since equations (2.1) are linear, the disturbances satisfy the same equations. Therefore,

$$\frac{\partial \tilde{u_r}}{\partial r} + \frac{\tilde{u_r}}{r} + \frac{1}{r}\frac{\partial \tilde{u_\theta}}{\partial \theta} = 0, \quad \frac{\partial \tilde{p}}{\partial r} = -\mu \tilde{u_r}, \quad \frac{1}{r}\frac{\partial \tilde{p}}{\partial \theta} = -\mu \tilde{u_\theta}. \tag{2.2}$$

We use separation of variables and assume that the disturbances are of the form

$$(\tilde{u_r}, \tilde{u_\theta}, \tilde{p}) = (f(r), \tau(r), \psi(r))g(t)e^{in\theta}. \tag{2.3}$$

Using (2.3) in equation (2.2) yields the following ordinary differential equation for $f(r)$:

$$\left(r^3 f'(r)\right)' - \left(n^2 - 1\right) r f(r) = 0. \tag{2.4}$$

The above equation is exact meaning there has been no linearization of any sort up until now. Next we derive the boundary conditions for this equation from linearization of the interfacial dynamic boundary conditions. Let the disturbance of the inner interface be of the form $a = A_n(t)e^{in\theta}$ and the disturbance of the outer interface be $b = B_n(t)e^{in\theta}$. Using the ansatz (2.3), the linearized kinematic conditions at the interfaces are given by

$$\frac{dA_n(t)}{dt} = f(R_0)g(t) - A_n(t)\frac{Q}{2\pi R_0^2}, \qquad \frac{dB_n(t)}{dt} = f(R_1)g(t) - B_n(t)\frac{Q}{2\pi R_1^2}. \tag{2.5}$$

Next, we consider the linearized dynamic interface condition (see equation (10) in Gin

& Daripa (2015)). At the inner interface, this is

$$\begin{aligned}&\Big\{f(R_0)(\mu_i-\mu_1)+R_0\big[\mu_i(f^-)'(R_0)-\mu_1(f^+)'(R_0)\big]\Big\}g(t)\\&=\left\{\frac{Qn^2}{2\pi R_0^2}(\mu_1-\mu_i)-T_0\frac{n^4-n^2}{R_0^3}\right\}A_n(t).\end{aligned}\tag{2.6}$$

where T_0 is the interfacial tension of the inner interface. The linearized dynamic condition at the outer interface is

$$\begin{aligned}&\Big\{f(R_1)(\mu_1-\mu_o)+R_1\big[\mu_1(f^-)'(R_1)-\mu_o(f^+)'(R_1)\big]\Big\}g(t)\\&=\left\{\frac{Qn^2}{2\pi R_1^2}(\mu_o-\mu_1)-T_1\frac{n^4-n^2}{R_1^3}\right\}B_n(t).\end{aligned}\tag{2.7}$$

where T_1 is the interfacial tension of the outer interface. The derivative terms in (2.6) and (2.7) can be replaced by using the fact that $f(r)$ is a solution to equation (2.4). This results in the following system of equations.

$$\widetilde{\mathbf{M}}_1\begin{pmatrix}f(R_0)g(t)\\f(R_1)g(t)\end{pmatrix}=\begin{pmatrix}F_0A_n(t)\\F_1B_n(t)\end{pmatrix},\tag{2.8}$$

where

$$\widetilde{\mathbf{M}}_1=\begin{pmatrix}\mu_i-\mu_1\frac{\left(\frac{R_0}{R_1}\right)^{2n}+1}{\left(\frac{R_0}{R_1}\right)^{2n}-1} & 2\mu_1\frac{\left(\frac{R_0}{R_1}\right)^{n-1}}{\left(\frac{R_0}{R_1}\right)^{2n}-1}\\ 2\mu_1\frac{\left(\frac{R_0}{R_1}\right)^{n+1}}{\left(\frac{R_0}{R_1}\right)^{2n}-1} & \mu_o-\mu_1\frac{\left(\frac{R_0}{R_1}\right)^{2n}+1}{\left(\frac{R_0}{R_1}\right)^{2n}-1}\end{pmatrix},\tag{2.9}$$

and

$$F_0=\frac{Qn}{2\pi R_0^2}(\mu_1-\mu_i)-T_0\frac{n^3-n}{R_0^3},\qquad F_1=\frac{Qn}{2\pi R_1^2}(\mu_o-\mu_1)-T_1\frac{n^3-n}{R_1^3}.\tag{2.10}$$

Using equation (2.8) in the kinematic condition (2.5),

$$\frac{d}{dt}\begin{pmatrix}A_n(t)\\B_n(t)\end{pmatrix}=\widetilde{\mathbf{M}}_1^{-1}\begin{pmatrix}A_n(t)\\B_n(t)\end{pmatrix}-\frac{Q}{2\pi}\begin{pmatrix}\frac{1}{R_0^2}&0\\0&\frac{1}{R_1^2}\end{pmatrix}\begin{pmatrix}A_n(t)\\B_n(t)\end{pmatrix}=:\mathbf{M}_1(t)\begin{pmatrix}A_n(t)\\B_n(t)\end{pmatrix},\tag{2.11}$$

where $\mathbf{M}_1(t)$ is the 2×2 matrix with entries indexed by $i, j = 0, 1$ given by

$$\begin{aligned}
\Big(\mathbf{M}_1(t)\Big)_{00} &= \frac{\left\{(\mu_o+\mu_1) - (\mu_o-\mu_1)\left(\frac{R_0}{R_1}\right)^{2n}\right\} F_0}{(\mu_1-\mu_i)(\mu_o-\mu_1)\left(\frac{R_0}{R_1}\right)^{2n} + (\mu_1+\mu_i)(\mu_o+\mu_1)} - \frac{Q}{2\pi R_0^2}, \\
\Big(\mathbf{M}_1(t)\Big)_{01} &= \frac{2\mu_1\left(\frac{R_0}{R_1}\right)^{n-1} F_1}{(\mu_1-\mu_i)(\mu_o-\mu_1)\left(\frac{R_0}{R_1}\right)^{2n} + (\mu_1+\mu_i)(\mu_o+\mu_1)}, \\
\Big(\mathbf{M}_1(t)\Big)_{10} &= \frac{2\mu_1\left(\frac{R_0}{R_1}\right)^{n+1} F_0}{(\mu_1-\mu_i)(\mu_o-\mu_1)\left(\frac{R_0}{R_1}\right)^{2n} + (\mu_1+\mu_i)(\mu_o+\mu_1)}, \\
\Big(\mathbf{M}_1(t)\Big)_{11} &= \frac{\left\{(\mu_1+\mu_i) + (\mu_1-\mu_i)\left(\frac{R_0}{R_1}\right)^{2n}\right\} F_1}{(\mu_1-\mu_i)(\mu_o-\mu_1)\left(\frac{R_0}{R_1}\right)^{2n} + (\mu_1+\mu_i)(\mu_o+\mu_1)} - \frac{Q}{2\pi R_1^2}.
\end{aligned} \tag{2.12}$$

This matrix can be found in Beeson-Jones & Woods (2015). However, the derivation of the matrix here differs from the approach taken there. In particular, Beeson-Jones & Woods (2015) make use of the potential function formulation. The present formulation uses the function $f(r)$ which satisfies the ODE (2.4). There are two main advantages to this approach. One is that the variational form of (2.4) can be used to obtain upper bounds on the eigenvalues of the matrix $\mathbf{M}_1$. This is done by Gin & Daripa (2015). The other advantage is that this approach can be extended to flows that have variable viscosity fluids. This has been done for rectilinear flows by Daripa (see for example Daripa (2008*a*)) and will be performed for radial flow in an upcoming work.

3. Eigenvalues and Eigenvectors of $\mathbf{M}_1$

Of particular importance are the eigenvalues and eigenvectors of the matrix $\mathbf{M}_1(t)$. The matrix will have two eigenvalues (counted with multiplicity) in $\mathbb{C}$. Although the derivation is different, exact expressions for the eigenvalues are given in Gin & Daripa (2015) and are denoted by $\sigma^+(t)$ and $\sigma^-(t)$. Let the eigenvectors associated with these eigenvalues be denoted by

$$\begin{pmatrix} A_n^+(t) \\ B_n^+(t) \end{pmatrix}, \qquad \begin{pmatrix} A_n^-(t) \\ B_n^-(t) \end{pmatrix}.$$

Then

$$\frac{d}{dt}\begin{pmatrix} A_n^\pm(t) \\ B_n^\pm(t) \end{pmatrix} = \mathbf{M}_1(t)\begin{pmatrix} A_n^\pm(t) \\ B_n^\pm(t) \end{pmatrix} = \sigma^\pm(t)\begin{pmatrix} A_n^\pm(t) \\ B_n^\pm(t) \end{pmatrix},$$

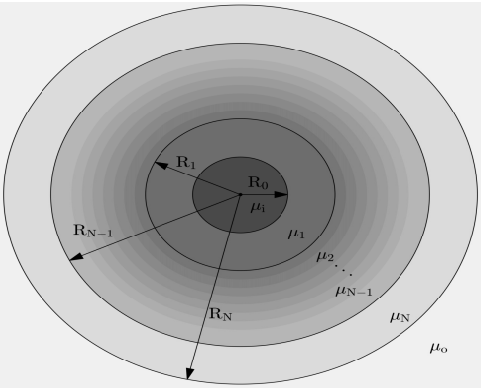

Figure 2: The basic solution for N-layer flow

which means that

$$\frac{dA_n^{\pm}(t)}{dt} = \sigma^{\pm}(t)A_n^{\pm}(t), \qquad \frac{dB_n^{\pm}(t)}{dt} = \sigma^{\pm}(t)B_n^{\pm}(t). \tag{3.1}$$

Using (3.1) in equation (2.5),

$$A_n^{\pm}(t) = \frac{f^{\pm}(R_0)}{\sigma^{\pm}(t) + \frac{Q}{2\pi R_0^2}} g^{\pm}(t), \qquad B_n^{\pm}(t) = \frac{f^{\pm}(R_1)}{\sigma^{\pm}(t) + \frac{Q}{2\pi R_1^2}} g^{\pm}(t). \tag{3.2}$$

Equation (3.2) defines the eigenvectors of $\mathbf{M}_1$. Since the eigenvectors are defined only up to a constant, we can take WLOG

$$\begin{pmatrix} A_n^+(t) \\ B_n^+(t) \end{pmatrix} = \begin{pmatrix} \left(\frac{f^+(R_0)}{f^+(R_1)}\right)\left(\sigma^+(t) + \frac{Q}{2\pi R_1^2}\right) \\ \sigma^+(t) + \frac{Q}{2\pi R_0^2} \end{pmatrix}, \begin{pmatrix} A_n^-(t) \\ B_n^-(t) \end{pmatrix} = \begin{pmatrix} \left(\frac{f^-(R_0)}{f^-(R_1)}\right)\left(\sigma^-(t) + \frac{Q}{2\pi R_1^2}\right) \\ \sigma^-(t) + \frac{Q}{2\pi R_0^2} \end{pmatrix}. \tag{3.3}$$

Using equation $(3.2)_1$ in the first component of equation (2.8),

$$\frac{f^{\pm}(R_0)}{f^{\pm}(R_1)} = \frac{2\left(\sigma^{\pm}(t) + \frac{Q}{2\pi R_0^2}\right)\mu_1\left(\frac{R_0}{R_1}\right)^{n-1}}{\left(\sigma^{\pm}(t) + \frac{Q}{2\pi R_0^2}\right)\left(\left(\frac{R_0}{R_1}\right)^{2n}(\mu_1 - \mu_i) + (\mu_1 + \mu_i)\right) + F_0\left\{\left(\frac{R_0}{R_1}\right)^{2n} - 1\right\}}. \tag{3.4}$$

By using this expression with (3.3), the eigenvectors can be found once the eigenvalues are known. In the numerical results that follow in §6, the ODE (2.11) is solved by expanding the disturbance in terms of the time-dependent eigenvectors of $\mathbf{M}_1$, given by equation (3.3), at each time step.

4. Multi-Layer Flow

The derivation in §2 can be extended to flows with an arbitrary number of fluid layers. Consider a flow in which there are N internal layers with $N + 1$ interfaces located at

$R = R_j$, $j = 0, ..., N$. Let the disturbance of the interface located at R_j be given by $A_n^j(t)e^{in\theta}$. The linearized kinematic interface conditions are given by

$$\frac{dA_n^j(t)}{dt} = f(R_i)g(t) - A_n^j(t)\frac{Q}{2\pi R_j^2}. \tag{4.1}$$

The linearized dynamic interface condition at the inner interface ($R = R_0$) is

$$\begin{aligned} &\Big\{f(R_0)(\mu_i - \mu_1) + R_0\big[\mu_i(f^-)'(R_0) - \mu_1(f^+)'(R_0)\big]\Big\}g(t) \\ =&\left\{\frac{Qn^2}{2\pi R_0^2}(\mu_1 - \mu_i) - T_0\frac{n^4 - n^2}{R_0^3}\right\}A_n^0(t). \end{aligned} \tag{4.2}$$

The linearized dynamic condition at the outer interface is

$$\begin{aligned} &\Big\{f(R_N)(\mu_N - \mu_o) + R_N\big[\mu_N(f^-)'(R_N) - \mu_o(f^+)'(R_N)\big]\Big\}g(t) \\ =&\left\{\frac{Qn^2}{2\pi R_N^2}(\mu_o - \mu_N) - T_N\frac{n^4 - n^2}{R_N^3}\right\}A_n^N(t). \end{aligned} \tag{4.3}$$

For any intermediate interface at $R = R_j$, the dynamic condition is

$$\begin{aligned} &\Big\{f(R_j)(\mu_j - \mu_{j+1}) + R_j\big[\mu_j(f^-)'(R_j) - \mu_{j+1}(f^+)'(R_j)\big]\Big\}g(t) \\ =&\left\{\frac{Qn^2}{2\pi R_j^2}(\mu_{j+1} - \mu_j) - T_j\frac{n^4 - n^2}{R_j^3}\right\}A_n^j(t). \end{aligned} \tag{4.4}$$

Using the fact that $f(r)$ is a solution to the differential equation (2.4), the dynamic interface condition (4.2) at the inner interface becomes

$$\left\{\mu_i - \mu_1\frac{\left(\frac{R_0}{R_1}\right)^{2n} + 1}{\left(\frac{R_0}{R_1}\right)^{2n} - 1}\right\}f(R_0)g(t) + 2\mu_1\frac{\left(\frac{R_0}{R_1}\right)^{n-1}}{\left(\frac{R_0}{R_1}\right)^{2n} - 1}f(R_1)g(t) = F_0A_n^0(t), \tag{4.5}$$

where

$$F_0 = \frac{Qn}{2\pi R_0^2}(\mu_1 - \mu_i) - T_0\frac{n^3 - n}{R_0^3}. \tag{4.6}$$

Similarly, the dynamic interface condition (4.3) for the outer interface reduces to

$$\left\{\mu_o - \mu_N\frac{\left(\frac{R_{N-1}}{R_N}\right)^{2n} + 1}{\left(\frac{R_{N-1}}{R_N}\right)^{2n} - 1}\right\}f(R_N)g(t) + 2\mu_N\frac{\left(\frac{R_{N-1}}{R_N}\right)^{n+1}}{\left(\frac{R_{N-1}}{R_N}\right)^{2n} - 1}f(R_{N-1})g(t) = F_NA_n^N(t), \tag{4.7}$$

where

$$F_N = \frac{Qn}{2\pi R_N^2}(\mu_o - \mu_N) - T_N\frac{n^3 - n}{R_N^3}, \tag{4.8}$$

and the dynamic interface conditions at the intermediate interfaces is

$$\begin{aligned}
&\left\{-\mu_j \frac{\left(\frac{R_{j-1}}{R_j}\right)^{2n}+1}{\left(\frac{R_{j-1}}{R_j}\right)^{2n}-1} - \mu_{j+1}\frac{\left(\frac{R_j}{R_{j+1}}\right)^{2n}+1}{\left(\frac{R_j}{R_{j+1}}\right)^{2n}-1}\right\} f(R_j)g(t) \\
&+ 2\mu_j \frac{\left(\frac{R_{j-1}}{R_j}\right)^{n+1}}{\left(\frac{R_{j-1}}{R_j}\right)^{2n}-1} f(R_{j-1})g(t) + 2\mu_{j+1}\frac{\left(\frac{R_j}{R_{j+1}}\right)^{n-1}}{\left(\frac{R_j}{R_{j+1}}\right)^{2n}-1} f(R_{j+1})g(t) \\
&= F_j A_n^j(t).
\end{aligned} \tag{4.9}$$

where

$$F_j = \frac{Qn}{2\pi R_j^2}(\mu_{j+1}-\mu_j) - T_j\frac{n^3-n}{R_j^3}. \tag{4.10}$$

Equations (4.5), (4.7), and (4.9) can be written as a system of equations of the form

$$\widetilde{\mathbf{M}}_N \begin{pmatrix} f(R_0)g(t) \\ \vdots \\ f(R_N)g(t) \end{pmatrix} = \begin{pmatrix} F_0 A_n^0(t) \\ \vdots \\ F_N A_n^N(t) \end{pmatrix},$$

where $\widetilde{\mathbf{M}}_N$ is the $(N+1)\times(N+1)$ tridiagonal matrix with entries indexed by $i,j = 0,...N$ given by

$$\begin{aligned}
\left(\widetilde{\mathbf{M}}_N\right)_{00} &= \mu_i - \mu_1\frac{\left(\frac{R_0}{R_1}\right)^{2n}+1}{\left(\frac{R_0}{R_1}\right)^{2n}-1}, \qquad \left(\widetilde{\mathbf{M}}_N\right)_{01} = 2\mu_1\frac{\left(\frac{R_0}{R_1}\right)^{n-1}}{\left(\frac{R_0}{R_1}\right)^{2n}-1} \\
\left(\widetilde{\mathbf{M}}_N\right)_{j,j-1} &= 2\mu_j\frac{\left(\frac{R_{j-1}}{R_j}\right)^{n+1}}{\left(\frac{R_{j-1}}{R_j}\right)^{2n}-1}, \\
\left(\widetilde{\mathbf{M}}_N\right)_{j,j} &= -\mu_j\frac{\left(\frac{R_{j-1}}{R_j}\right)^{2n}+1}{\left(\frac{R_{j-1}}{R_j}\right)^{2n}-1} - \mu_{j+1}\frac{\left(\frac{R_j}{R_{j+1}}\right)^{2n}+1}{\left(\frac{R_j}{R_{j+1}}\right)^{2n}-1}, \\
\left(\widetilde{\mathbf{M}}_N\right)_{j,j+1} &= 2\mu_{j+1}\frac{\left(\frac{R_j}{R_{j+1}}\right)^{n-1}}{\left(\frac{R_j}{R_{j+1}}\right)^{2n}-1}, \\
\left(\widetilde{\mathbf{M}}_N\right)_{N,N-1} &= 2\mu_N\frac{\left(\frac{R_{N-1}}{R_N}\right)^{n+1}}{\left(\frac{R_{N-1}}{R_N}\right)^{2n}-1}, \qquad \left(\widetilde{\mathbf{M}}_N\right)_{N,N} = \mu_o - \mu_N\frac{\left(\frac{R_{N-1}}{R_N}\right)^{2n}+1}{\left(\frac{R_{N-1}}{R_N}\right)^{2n}-1}.
\end{aligned} \tag{4.11}$$

Combining this system of equations with the linearized kinematic interface conditions yields

$$\frac{d}{dt}\begin{pmatrix} A_n^0(t) \\ \vdots \\ A_n^N(t) \end{pmatrix} = \mathbf{M}_N \begin{pmatrix} A_n^0(t) \\ \vdots \\ A_n^N(t) \end{pmatrix}, \tag{4.12}$$

where

$$\mathbf{M}_N = \widetilde{\mathbf{M}}_N^{-1} \begin{pmatrix} F_0 & \dots & 0 \\ \vdots & \ddots & \vdots \\ 0 & \dots & F_N \end{pmatrix} - \frac{Q}{2\pi} \begin{pmatrix} \frac{1}{R_0^2} & \dots & 0 \\ \vdots & \ddots & \vdots \\ 0 & \dots & \frac{1}{R_N^2} \end{pmatrix} \tag{4.13}$$

For the particular case of $N = 1$ (i.e. three-layer flow), equation (4.13) reduces to the matrix given by equation (2.12).

5. Time dependent injection rate

Traditionally, the injection rate Q for a radial Hele-Shaw flow is taken to be constant. However, in the formulation above, the injection rate can be taken to be a function of time. There have been many studies that have explored the implications of using a strategically chosen time-dependent injection rate (see for example Beeson-Jones & Woods (2015), Dias *et al.* (2012), Li *et al.* (2009), and Zheng *et al.* (2015)). Almost all of these studies are for two-layer flows with the exception of Beeson-Jones & Woods (2015) who consider three-layer flows. In this section, we extend some of these results to multi-layer flows and also present some new results for time-dependent injection rates for three-layer flows.

5.1. *Two-layer flow*

In order to set the stage for time-dependent injection rates for multi-layer flows, we review some results for two-layer flows. In particular, there is a time-dependent maximum injection rate for which the flow is stable. There is another time-dependent injection rate for which the most dangerous wave number is constant for all time. We derive these below.

Consider the growth rate for two-layer radial Hele-Shaw flows. From Gin & Daripa (2015), it is given by the expression

$$\sigma = \frac{Qn}{2\pi R^2}\frac{\mu_o - \mu_i}{\mu_o + \mu_i} - \frac{Q}{2\pi R^2} - \frac{T}{\mu_o + \mu_i}\frac{n\left(n^2-1\right)}{R^3}, \tag{5.1}$$

where $R = R(t)$ depends on time. A disturbance with wave number n is stable if $\sigma \leqslant 0$. This condition is equivalent to

$$Q \leqslant \frac{1}{R} \frac{2\pi T n \left(n^2 - 1\right)}{n(\mu_o - \mu_i) - (\mu_o + \mu_i)}. \tag{5.2}$$

Therefore, as derived in Beeson-Jones & Woods (2015), the maximum injection rate for which the disturbance with wave number n is stable is

$$Q = \frac{1}{R} \frac{2\pi T n \left(n^2 - 1\right)}{n(\mu_o - \mu_i) - (\mu_o + \mu_i)}. \tag{5.3}$$

The maximum injection rate for which the flow is stable is found by taking the minimum of equation (5.3) over all values of n. It is shown in Beeson-Jones & Woods (2015) that for $t >> 1$, the maximum injection rate for which the flow is stable behaves like $Q \propto t^{-1/3}$. For applications like oil recovery, it is beneficial to stabilize the flow, but it is also cost effective to inject as fast as possible. Therefore, the use of the maximum injection rate for which the flow is stable is advantageous for oil recovery applications.

Returning to the equation (5.1), the wave number $n = n_m$ with maximum growth rate is easily found by taking the derivative of this function with respect to n and setting it equal to zero. The relationship between n_m and the injection rate Q is given by

$$\frac{QR}{2\pi T}(\mu_o - \mu_i) = 3n_m^2 - 1. \tag{5.4}$$

It follows that $n_m = \sqrt{QR(\mu_o - \mu_i)/(6\pi T) + 1/3}$ is independent of time if a time-dependent injection rate $Q(t)$ is chosen so that QR is independent of time. The injection rate which achieves this is of the form $Q(t) \propto t^{-1/3}$. This is a classical result and can be found, among other places, as a special case of the result by Zheng *et al.* (2015). The growth rate corresponding to this wave number could be positive or negative depending on the values of the parameters. When positive, it is the most dangerous wave number. If this is the case, then n_m gives the number of fingers which will eventually form. As seen in the numerical experiments done by Li *et al.* (2009), this is independent of the initial conditions that are chosen. This stands in contrast to the case of a constant injection rate in which n_m increases with time. This cascade to higher modes is implied by the above formula for the n_m and is also observed in experiments by Cardoso & Woods (1995).

5.2. *Maximum Injection Rate for a Stable Flow*

We now wish to obtain a result analogous to equation (5.3) but for multi-layer flows. An exact expression like equation (5.3) is not feasible in this case, so instead we look for bounds that ensure stability of the flow.

5.2.1. *Three-layer Flow*

We start by considering three-layer flow. By Gershgorin's Circle Theorem, all of the eigenvalues of $\mathbf{M}_1$ will have a negative real part if the following two inequalities hold

$$\begin{aligned}
\frac{Q}{2\pi R_0^2} \geqslant & \frac{\left\{(\mu_o+\mu_1)-(\mu_o-\mu_1)\left(\frac{R_0}{R_1}\right)^{2n}\right\}F_0}{(\mu_1-\mu_i)(\mu_o-\mu_1)\left(\frac{R_0}{R_1}\right)^{2n}+(\mu_1+\mu_i)(\mu_o+\mu_1)} \\
& + \frac{2\mu_1\left(\frac{R_0}{R_1}\right)^{n-1}F_1}{(\mu_1-\mu_i)(\mu_o-\mu_1)\left(\frac{R_0}{R_1}\right)^{2n}+(\mu_1+\mu_i)(\mu_o+\mu_1)}, \\
\frac{Q}{2\pi R_1^2} \geqslant & \frac{\left\{(\mu_1+\mu_i)+(\mu_1-\mu_i)\left(\frac{R_0}{R_1}\right)^{2n}\right\}F_1}{(\mu_1-\mu_i)(\mu_o-\mu_1)\left(\frac{R_0}{R_1}\right)^{2n}+(\mu_1+\mu_i)(\mu_o+\mu_1)} \\
& + \frac{2\mu_1\left(\frac{R_0}{R_1}\right)^{n+1}F_0}{(\mu_1-\mu_i)(\mu_o-\mu_1)\left(\frac{R_0}{R_1}\right)^{2n}+(\mu_1+\mu_i)(\mu_o+\mu_1)}.
\end{aligned} \tag{5.5}$$

Recall from equation (2.10) that both F_0 and F_1 depend on Q. By using (2.10) in equation (5.5) and solving for Q, the following condition on the injection rate can be found which is sufficient to ensure that the eigenvalues of $\mathbf{M}_1$ have a negative real part.

$$Q \leqslant \min\{G_0, G_1\}, \tag{5.6}$$

where

$$G_0 = \frac{2\pi T_0}{R_0}\frac{(n^3-n)D_0}{nD_1-D_2}, \tag{5.7}$$

$$G_1 = \frac{2\pi T_1}{R_1}\frac{(n^3-n)D_3}{nD_4-D_2}, \tag{5.8}$$

$$D_0 = (\mu_o+\mu_1)+2\mu_1\left(\frac{T_1}{T_0}\right)\left(\frac{R_0}{R_1}\right)^{n+2}-(\mu_o-\mu_1)\left(\frac{R_0}{R_1}\right)^{2n}, \tag{5.9}$$

$$D_1 = (\mu_o+\mu_1)(\mu_1-\mu_i)+2\mu_1(\mu_o-\mu_1)\left(\frac{R_0}{R_1}\right)^{n+1}-(\mu_o-\mu_1)(\mu_1-\mu_i)\left(\frac{R_0}{R_1}\right)^{2n}, \tag{5.10}$$

$$D_2 = (\mu_o+\mu_1)(\mu_1+\mu_i)+(\mu_o-\mu_1)(\mu_1-\mu_i)\left(\frac{R_0}{R_1}\right)^{2n}, \tag{5.11}$$

$$D_3 = (\mu_1+\mu_i)+2\mu_1\left(\frac{T_0}{T_1}\right)\left(\frac{R_0}{R_1}\right)^{n-2}+(\mu_1-\mu_i)\left(\frac{R_0}{R_1}\right)^{2n}, \tag{5.12}$$

$$D_4 = (\mu_o-\mu_1)(\mu_1+\mu_i)+2\mu_1(\mu_1-\mu_i)\left(\frac{R_0}{R_1}\right)^{n-1}+(\mu_o-\mu_1)(\mu_1-\mu_i)\left(\frac{R_0}{R_1}\right)^{2n}. \tag{5.13}$$

Therefore, the flow is stable if Q satisfies (5.6) for all n. Note that the only terms in the expressions for G_0 and G_1 that are time-dependent are R_0 and R_1. As time increases, the interfaces become closer together and $R_0/R_1 \to 1$ as $t \to \infty$. Therefore, from equations (5.7) and (5.8), $G_0 \propto 1/R_0$ and $G_1 \propto 1/R_1$ as $t \to \infty$. This is precisely the relationship between Q and R in equation (5.3). Therefore, $G_0 \propto t^{-1/3}$ and $G_1 \propto t^{-1/3}$ for $t >> 1$.

5.2.2. *Limiting Cases*

We now investigate the upper bound (5.6) in two limiting cases - when the intermediate layer is thin ($R_0/R_1 \to 1$) and when the intermediate layer is thick ($R_0/R_1 \to 0$).

First we consider the thin-layer limit. Note that for any three-layer Hele-Shaw flow, the distance between the interfaces decreases with time. Therefore, even if the interfaces are initially far apart, the intermediate layer will eventually become thin. In the limit as $R_0/R_1 \to 1$, equation (5.7) becomes

$$\lim_{\frac{R_0}{R_1}\to 1} G_0 = \frac{2\pi}{R_0}\frac{(n^3-n)(T_0+T_1)}{n(\mu_o-\mu_i)-(\mu_o+\mu_i)}. \tag{5.14}$$

Likewise,

$$\lim_{\frac{R_0}{R_1}\to 1} G_1 = \frac{2\pi}{R_1}\frac{(n^3-n)(T_0+T_1)}{n(\mu_o-\mu_i)-(\mu_o+\mu_i)}. \tag{5.15}$$

Since we are considering the limit as $R_0/R_1 \to 1$, it is also true that $R_0 \to R_1$. If we denote $R := R_1$, then

$$\lim_{\frac{R_0}{R_1}\to 1} G_0 = \lim_{\frac{R_0}{R_1}\to 1} G_1 = \frac{2\pi}{R}\frac{(n^3-n)(T_0+T_1)}{n(\mu_o-\mu_i)-(\mu_o+\mu_i)},$$

and the upper bound (5.6) becomes

$$Q \leqslant \frac{2\pi}{R}\frac{(n^3-n)(T_0+T_1)}{n(\mu_o-\mu_i)-(\mu_o+\mu_i)}. \tag{5.16}$$

After some algebraic manipulation, this condition becomes

$$\frac{Qn}{2\pi R^2}\frac{\mu_o-\mu_i}{\mu_o+\mu_i} - \frac{Q}{2\pi R^2} - \frac{(T_0+T_1)}{\mu_o+\mu_i}\frac{(n^3-n)}{R^3} \leqslant 0. \tag{5.17}$$

The term on the left-hand side is precisely the two-layer growth rate for a single interface with interfacial tension $T_0 + T_1$. This is the same thin-layer limit that was found for the exact three-layer growth rate by Gin & Daripa (2015).

We now investigate the thick-layer limit ($R_0 << R_1$).

$$\lim_{\frac{R_0}{R_1}\to 0} G_0 = \frac{2\pi T_0}{R_0}\frac{n^3-n}{n(\mu_1-\mu_i)-(\mu_1+\mu_i)}, \tag{5.18}$$

and for $n > 2$,

$$\lim_{\frac{R_0}{R_1}\to 0} G_1 = \frac{2\pi T_1}{R_1}\frac{n^3-n}{n(\mu_o-\mu_1)-(\mu_o+\mu_1)}. \tag{5.19}$$

Notice that in this limit, G_0 only contains terms associated with the inner interface and G_1 only contains terms associated with the outer interface. After some algebraic manipulation, the condition that $Q \leqslant G_0$ becomes

$$\frac{Qn}{2\pi R_0^2}\frac{\mu_1-\mu_i}{\mu_1+\mu_i} - \frac{Q}{2\pi R_0^2} - \frac{T_0}{\mu_1+\mu_i}\frac{(n^3-n)}{R_0^3} \leqslant 0. \tag{5.20}$$

This is the condition that the inner interface is stable according to its two-layer growth rate. Similarly, the condition that $Q \leqslant G_1$ leads to

$$\frac{Qn}{2\pi R_1^2}\frac{\mu_o-\mu_1}{\mu_o+\mu_1} - \frac{Q}{2\pi R_1^2} - \frac{T_1}{\mu_o+\mu_1}\frac{(n^3-n)}{R_1^3} \leqslant 0, \tag{5.21}$$

which is the condition that the outer interface is stable according to its two-layer growth rate. Therefore, as expected, in the limit of a thick intermediate layer the interfaces are decoupled and the flow is stable if each interface is individually stable.

5.2.3. *Multi-layer Flow*

We now find sufficient conditions on the injection rate to stabilize a flow with an arbitrary number of fluid layers. The approach used for three-layer flows in §5.2.1 which uses Gershgorin's circle theorem can be adapted to flows with four or more layers by calculating the corresponding matrix $\mathbf{M}_N$. However, for the sake of simplicity, we adopt a different approach. In Gin & Daripa (2015, p.22), upper bounds are found on the real part of the growth rate for flows with N internal layers by using the variational form of the problem. This upper bound is the maximum of $N+1$ expressions, each of which has terms that pertain to the parameter values at one of the interfaces. From examining the upper bound, it can be seen that a disturbance with wave number n will be stable if $E_j \leqslant 0$ for $j = 0, 1, ..., N$ where E_j is related to F_j (see equations (4.6), (4.8), and (4.10)) in the following way

$$E_0 = nR_0^2F_0 - \frac{Qn}{2\pi}\mu_i, \quad E_j = nR_j^2F_j, \quad \text{for } j = 1, ..., N-1, \quad E_N = nR_N^2F_N - \frac{Qn}{2\pi}\mu_o. \tag{5.22}$$

$E_j \leqslant 0$ for all j if

$$Q \leqslant \min\left\{\frac{1}{R_0}\frac{2\pi T_0 n(n^2-1)}{n(\mu_1-\mu_i)-\mu_i}, \min_{j=1,...,N-1}\frac{1}{R_j}\frac{2\pi T_j(n^2-1)}{\mu_{j+1}-\mu_j}, \frac{1}{R_N}\frac{2\pi T_N n(n^2-1)}{n(\mu_o-\mu_N)-\mu_o}\right\}. \tag{5.23}$$

Notice the similarity between the terms in (5.23) and the expression for two-layer flows given by equation (5.3).

5.3. *Choosing $Q(t)$ for a time-independent eigenvector of $\mathbf{M}_N$*

Note that the matrix $\mathbf{M}_1$ for three-layer flow is time-dependent (see equation (2.12)). Therefore, the eigenvalues and eigenvectors evolve in time. However, it is possible to have an eigenvector which persists for all time if a time-dependent injection rate is chosen cleverly. Recall from equation $(2.10)_1$ the expression for F_0 which the matrix $\mathbf{M}_1$ in (2.12) depends on:

$$F_0 = \frac{Qn}{2\pi R_0^2}(\mu_1 - \mu_i) - T_0\frac{n^3 - n}{R_0^3}.$$

If

$$Q(t) = \frac{2\pi T_0(n^2-1)}{R_0(t)(\mu_1 - \mu_i)}, \tag{5.24}$$

then $F_0 = 0$ for all t. This results in an injection rate of the form $Q(t) \propto t^{-1/3}$. If an injection rate of the form (5.24) is chosen, then the matrix $\mathbf{M}_1$ in (2.12) becomes

$$\mathbf{M}_1 = \begin{pmatrix} -\frac{Q}{2\pi R_0^2} & \frac{2\mu_1\left(\frac{R_0}{R_1}\right)^{n-1}F_1}{(\mu_1-\mu_i)(\mu_o-\mu_1)\left(\frac{R_0}{R_1}\right)^{2n}+(\mu_1+\mu_i)(\mu_o+\mu_1)} \\ 0 & \frac{\left\{(\mu_1+\mu_i)+(\mu_1-\mu_i)\left(\frac{R_0}{R_1}\right)^{2n}\right\}F_1}{(\mu_1-\mu_i)(\mu_o-\mu_1)\left(\frac{R_0}{R_1}\right)^{2n}+(\mu_1+\mu_i)(\mu_o+\mu_1)} - \frac{Q}{2\pi R_1^2} \end{pmatrix}.$$

Therefore, $\begin{pmatrix} 1 & 0 \end{pmatrix}^T$ is an eigenvector with an eigenvalue of $-Q/(2\pi R_0^2)$. If the initial condition is some constant multiple of this eigenvector (i.e. only the inner interface has a disturbance of wave number n), then the outer interface will stay circular and the disturbance of the inner interface will decay. This is true even if the outer interface individually is very unstable. Similarly, if the injection rate is chosen so that $F_1 = 0$, then $\begin{pmatrix} 0 & 1 \end{pmatrix}^T$ is an eigenvector with an eigenvalue of $-Q/(2\pi R_1^2)$. An initial condition in which only the outer interface has a disturbance of wave number n will result in the disturbance decaying and the inner interface remaining circular.

Note that this result can also be extended to flows with an arbitrary number of fluid layers. Recall that the expression for the matrix $\mathbf{M}_N$ is given by equation (4.13):

$$\mathbf{M}_N = \widetilde{\mathbf{M}}_N^{-1}\begin{pmatrix} F_0 & \dots & 0 \\ \vdots & \ddots & \vdots \\ 0 & \dots & F_N \end{pmatrix} - \frac{Q}{2\pi}\begin{pmatrix} \frac{1}{R_0^2} & \dots & 0 \\ \vdots & \ddots & \vdots \\ 0 & \dots & \frac{1}{R_N^2} \end{pmatrix}.$$

The formula for F_0 is the same as that for three-layer flow. Therefore, by using the

injection rate given by equation (5.24), $F_0 = 0$ for all t. Even without calculating the matrix $\widetilde{\mathbf{M}}_N^{-1}$, it is clear that $\begin{pmatrix} 1 & 0 & \cdots & 0 \end{pmatrix}^T$ is an eigenvector of $\mathbf{M}_N$ with eigenvalue $-Q/(2\pi R_0^2)$.

Similarly, we can use the expression (4.10) for F_j to find that using the injection rate

$$Q(t) = \frac{2\pi T_j (n^2 - 1)}{R_j(t)(\mu_{j+1} - \mu_j)} \tag{5.25}$$

will result in $F_j = 0$ for all t. There will be an eigenvector with a one in the jth position and zeros everywhere else, and the corresponding eigenvalue is $-Q/(2\pi R_j^2)$.

Note that in all of these cases, the time-independent eigenvector has a negative eigenvalue. Therefore, the span of the eigenvector is a stable manifold of the system. If the initial condition is such that only one interface is perturbed and the perturbation consists of only a single wave number and the injection rate is as prescribed by equation (5.25), the disturbance will decay. This is independent of the values of all of the parameters including viscosity and interfacial tension and is summarized in the following theorem.

THEOREM 1. *In any multi-layer radial Hele-Shaw flow, if all of the interfaces are circular except for one perturbed circular interface then there exists a time-dependent injection rate such that the circular interfaces remain circular and the disturbance on the perturbed interface decays.*

6. Numerical Results

In this section, we numerically investigate some interesting behavior of multi-layer flows by computing the motion of the interfaces within linear theory and calculating the growth rates of disturbances.

6.1. *Constant Injection Rate*

We start by considering flows with a constant injection rate. The motion of the interfaces is computed using the linear theory and the eigenvector expansion as described in §3 for three-layer radial flow. Analogous results can be obtained for flows with more than three layers using the formulation of §4, but we save that for future work. The values of the parameters can be found in the various figure captions below. Many of the plots below are graphs of the evolution of the amplitudes of a disturbance with wave number n for the inner interface (A_n) versus the outer interface (B_n). The '*' denotes

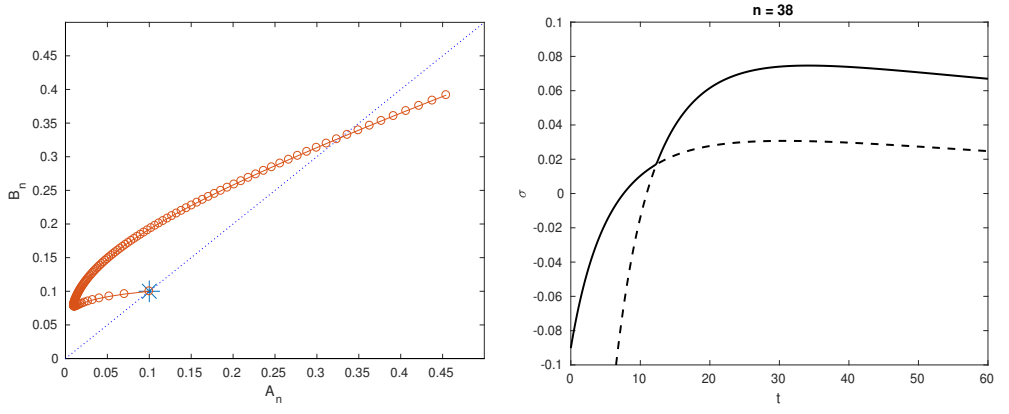

(a) (b)

Figure 3: A disturbance with a single wave number of $n = 38$ is given to both interfaces. Subfigure (a) shows the amplitude of the disturbance on the inner interface ($A_n(t)$) versus the amplitude of the disturbance of the outer interface ($B_n(t)$). Subfigure (b) is the eigenvalues of $\mathbf{M}_1$ versus time. The parameter values are $Q = 100, \mu_i = 2, \mu_1 = 6, \mu_o = 10, T_0 = T_1 = 1, R_0(0) = 15, R_1(0) = 20, n = 38, A_{38}(0) = B_{38}(0) = 0.1$.

the amplitudes at time $t = 0$. The markers on the line are equally spaced in time. The diagonal $A_n = B_n$ is given for reference.

We first investigate the behavior of a disturbance which consists of only a single wave number. An initial disturbance with wave number $n = 38$ is given to both interfaces with equal amplitude ($A_{38}(0) = B_{38}(0) = 0.1$). The initial disturbance is given by the (blue) '*' in Figure 3a. The value of the growth rates σ versus time are graphed in Figure 3b. Notice that initially both modes are stable, but then each in turn becomes unstable. Therefore, the disturbances will decay at first and then begin to grow. This is evident in Figure 3a since the line first moves toward the origin, meaning the disturbance amplitudes decay, but then moves away from the origin, meaning that the interfacial disturbances grow. Another interesting feature is that at first the disturbance on the outer interface is more unstable. However, near the end of the simulation the disturbance on the inner interface becomes more unstable. This occurs at the point where the curve crosses the diagonal in Figure 3a.

Figure 4 shows the case in which initially only the inner interface has a disturbance ($A_n \neq 0, B_n = 0$). According to the system of equations (2.11), the ODEs governing the interfaces are coupled. Therefore, we expect that the instability of the inner interface will

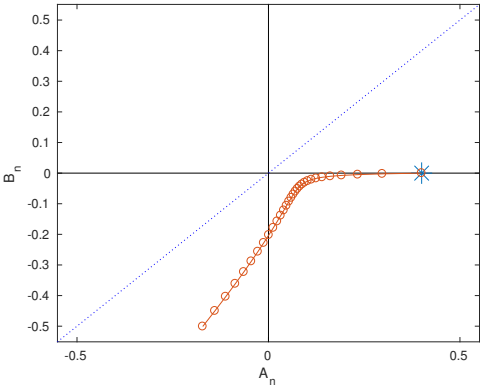

Figure 4: A plot of the amplitude of interfacial disturbances in the case that only the inner interface is disturbed initially. The parameter values are $Q = 100, \mu_i = 2, \mu_1 = 4, \mu_o = 10, T_0 = T_1 = 1, R_0(0) = 18, R_1(0) = 20, n = 30,\ A_{30}(0) = 0.4,\ B_{30}(0) = 0, 0 \leqslant t \leqslant 30$. Recall that $A_n(t)$ denotes the amplitude of the disturbance of the inner interface and $B_n(t)$ the outer interface.

be transferred to the outer interface at time $t > 0$. A disturbance immediately forms on the outer interface as the disturbance of the inner interface initially decays. An interesting thing to note is that as the disturbance develops on the outer interface (B_n), its sign is negative. Since the amplitude of the disturbance on the inner interface (A_n) is positive, this corresponds to disturbances that are out of phase. In the previous figures, the plots of A_n versus B_n were all in the first quadrant, which corresponds to in-phase disturbances. Another interesting feature of Figure 4 is that the curve eventually crosses the B_n-axis, meaning that the inner interface becomes circular, but then the disturbance of the inner interface begins to grow again but in phase with the disturbance of the outer interface.

In order to visualize the behavior of the interfaces, the interfaces corresponding to Figure 4 are plotted at three different times in Figure 5. The intermediate fluid that lies between the two interfaces is shaded grey. Because the disturbances are small compared to the radii of the unperturbed interfaces, zoomed in plots of the interfaces at each time step are given in Figure 6. Note that in Figure 6a, the outer interface is circular and only the inner interface has a disturbance. Figure 6b shows that the disturbances are out of phase at time $t = 15$. However, at time $t = 30$, the disturbances are in phase as illustrated in Figure 6c. Also, the outer interface which initially had no disturbance now has a larger disturbance than the inner interface.

In each of the previous figures, the perturbation of the circular interface initially

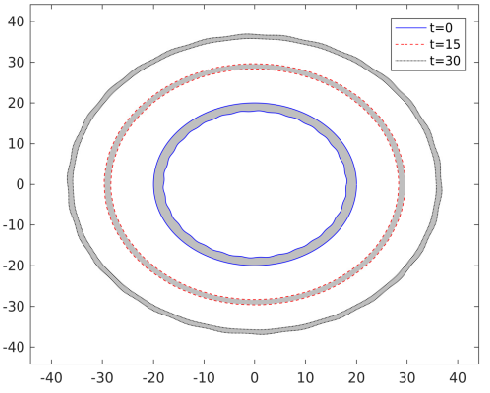

Figure 5: Plots of the interfaces in the case that only the inner interface is disturbed initially (see Figure 4). The interfaces are shown at times $t = 0$, $t = 15$, and $t = 30$.

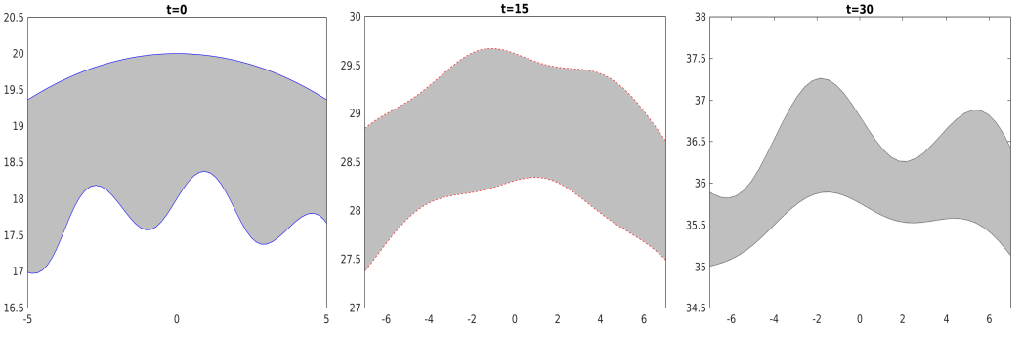

(a) (b) (c)

Figure 6: Plots of the interfaces in the case that only the inner interface is disturbed initially (see Figure 4). Only a segment of the middle layer is shown at three different time levels in order to show the wave patterns on the interfaces more clearly. The interfaces are shown at times (a) $t = 0$, (b) $t = 15$, and (c) $t = 30$.

contains only a single wave. A more interesting case is one in which the initial disturbance has several modes. In Figure 7, the initial disturbance on each interface is composed of three different wave numbers: $n = 6$, $n = 7$, and $n = 8$. The initial amplitudes of the disturbances are all the same. Plots of the maximum eigenvalue associated with each wave number are given in Figure 8. Note that at first $n = 6$ is the most unstable, then $n = 7$, and then $n = 8$. This cascade to higher modes is typical of radial Hele-Shaw flows. Figure 7a shows the evolution of the interfacial disturbances up to $t = 10$. Notice that at $t = 10$, the $n = 6$ disturbance has the largest amplitude. Figure 7b shows that the $n = 7$

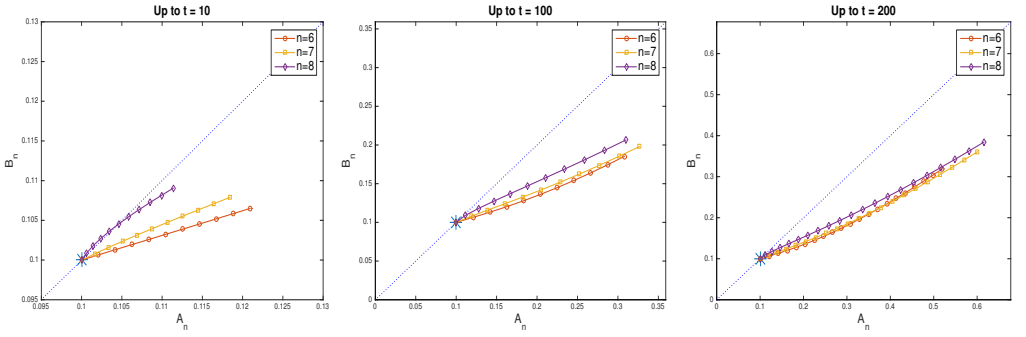

(a) (b) (c)

Figure 7: Plots of the amplitudes of interfacial disturbances in the case where the initial disturbance is composed of three different waves. Subfigure (a) shows the amplitudes for $0 \leqslant t \leqslant 10$, subfigure (b) for $0 \leqslant t \leqslant 100$, and subfigure (c) for $0 \leqslant t \leqslant 200$. The parameter values are $Q = 20, \mu_i = 2, \mu_1 = 5, \mu_o = 10, T_0 = T_1 = 1, R_0(0) = 10, R_1(0) = 20, n = 6, 7, 8, A_6(0) = B_6(0) = 0.1, A_7(0) = B_7(0) = 0.1, A_8(0) = B_8(0) = 0.1$. Recall that $A_n(t)$ denotes the amplitude of the disturbance of the inner interface and $B_n(t)$ the outer interface.

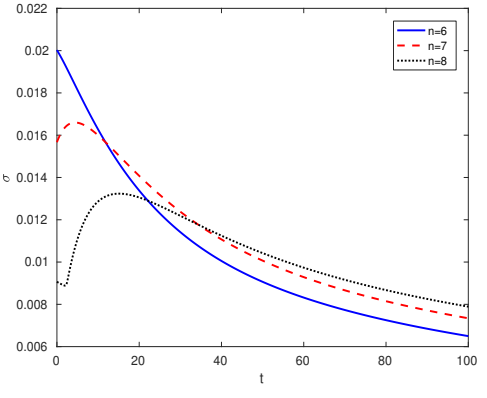

Figure 8: Plots of the maximum eigenvalue of $\mathbf{M}_1$ for three different wave numbers. The parameter values are $Q = 20, \mu_i = 2, \mu_1 = 5, \mu_o = 10, T_0 = T_1 = 1, R_0(0) = 10, R_1(0) = 20, n = 6, 7, 8$.

disturbance has the largest amplitude at $t = 100$, and Figure 7c shows that the $n = 8$ disturbance has the largest amplitude at $t = 200$.

6.2. *Time-dependent Injection Rate: Maximum Injection Rate for a Stable Flow*

We now consider flows with a time-dependent injection rate $Q(t)$. In this section we investigate the maximum value of the injection rate that results in a stable flow. This was studied analytically in §5. For two-layer radial flow, the maximum stable injection rate for a given wave number n and radius R of the circular interface is given exactly by the expression (5.3). By taking the minimum value over all wave numbers, a injection rate can be found which makes the flow stable. Note that in the expression (5.3), $Q(t)$ depends on $R(t)$. However, the position of the interface $R(t)$ also depends on the injection rate $Q(t)$. Therefore, even with the exact expression for $Q(t)$ in terms of $R(t)$, it is difficult to prescribe $Q(t)$ a priori. For the calculations that follow for two-layer flow, the injection rate is calculated from equation (5.3) using the initial position of the interface $R(0)$. Then we calculate the interfacial position $R(\Delta t)$ at the next time step Δt by using this injection rate. The process is then repeated for each time step.

In the figures that follow, a similar process is used to calculate the sufficient conditions for stabilization for three-layer flow given by equation (5.6) and for multi-layer flow given by equation (5.23). The injection rate is calculated by minimizing the expression (5.6) or (5.23) over all integer values of n and with the initial positions of the interfaces $R_j(0)$. Then the interfacial positions $R_j(\Delta t)$ at the next time step Δt are calculated using this injection rate and the process is repeated. To find the maximum stable flow rate for three-layer flow (see Figure 9), an additional calculation is needed. There is no analytical expression for the maximum stable flow rate for given values of n, R_0, and R_1 analogous to equation (5.3). Therefore, we use the expression for $\sigma^+(t)$ given in Gin & Daripa (2015). Newton's method is used to find the value of Q such that $\sigma^+(t) = 0$.

The maximum injection rate for which a certain two-layer flow is stable is given by the solid line in Figure 9. As a comparison, the maximum stable injection rate is calculated for three-layer flow in which the outer interface starts in the same position as the interface for two-layer flow, the viscosity of the inner and outer layers are the same as the two-layer flow, and the intermediate layer has a viscosity which is greater than the inner layer and smaller than the outer layer. This is the dashed line in Figure 9. Note that the three-layer flow is stable for a much larger injection rate due to the fact that the viscosity jumps at the interfaces are smaller. Also included in Figure 9 is the sufficient condition for stabilization given in equation (5.6). This is the dotted line in Figure 9. Note that for these particular values of the parameters, this bound, while not strict, allows for

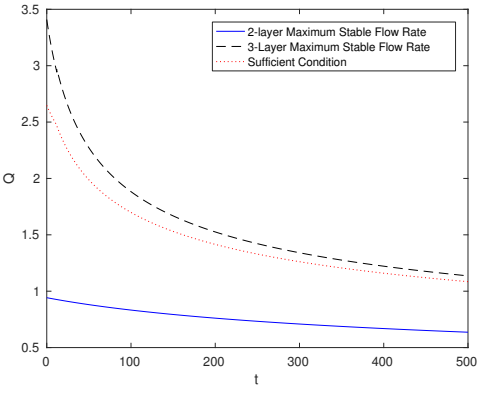

Figure 9: Plots of the maximum stable injection rate vs time for two-layer flow (solid line) and three-layer flow (dashed line) as well as the sufficient condition for stabilization given by equation (5.6) (dotted line). The values of the parameters are $\mu_i = 2$, $\mu_o = 10$, $T = 1$, $R(0) = 10$ for two-layer flow and $\mu_i = 2, \mu_1 = 6, \mu_o = 10, T_0 = T_1 = 1, R_0(0) = 8, R_1(0) = 10$ for three-layer flow.

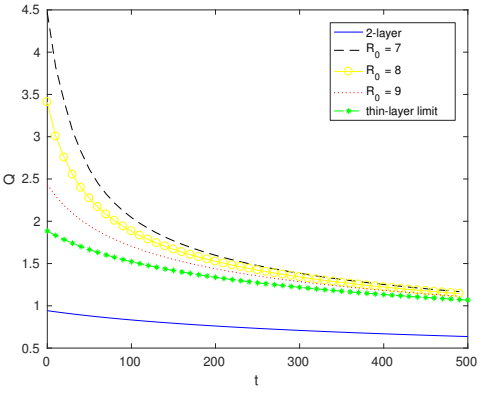

Figure 10: Plots of the maximum stable injection rate vs time for two-layer flow (solid line) and three-layer flow (dashed line) as well as the sufficient condition for stabilization given by equation (5.6). The values of the parameters are $\mu_i = 2$, $\mu_o = 10$, $T = 1$, $R(0) = 10$ for two-layer flow and $\mu_i = 2, \mu_1 = 6, \mu_o = 10, T_0 = T_1 = 1, R_0(0) = 7, 8, 9, R_1(0) = 10$ for three-layer flow.

a significant increase in the injection rate over two-layer flow. Like the equation (5.3) for two-layer flow, the sufficient condition for stabilization (5.6) is an expression which depends on the locations of the interfaces $R_0(t)$ and $R_1(t)$ which in turn depend on the injection rate $Q(t)$. Therefore, the injection rate $Q(t)$ cannot easily be determined a priori.

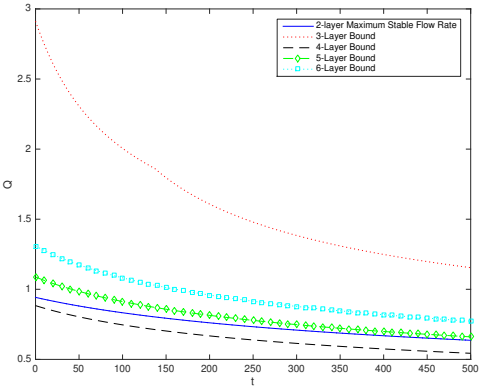

Figure 11: Plots of the maximum stable injection rate vs time for two-layer flow (solid line) as well as the sufficient condition for stabilization given by equation (5.6) for three-layer flow (dotted line) and the sufficient condition given by equation (5.23) for four, five, and six-layer flows. The values of the parameters are $\mu_i = 2$, $\mu_o = 10$, $T_j = 1$ for all j, $R_0(0) = 6$, and $R_N(0) = 10$. The interfaces are equally spaced at time $t = 0$ in all cases and the viscous jumps are the same at all interfaces.

In oil recovery applications, it is often expensive to include a more viscous intermediate fluid instead of just using water to displace oil. Therefore, it would be economically advantageous if a minimal amount of fluid could be used in the intermediate layer of a three-layer flow if it still allows the flow to be stabilized at a faster injection rate. This behavior is investigated in Figure 10. The solid line is the maximum stable injection rate for two-layer flow using the same parameters as in Figure 9. In particular, the initial position of the interface is $R(0) = 10$. This flow is compared with three-layer flows for which the outer interface is initially at $R_1(0) = 10$ and the inner interface is initially at $R_0(0) = 7, 8, 9$. Notice that as the middle layer becomes thinner, the maximum stable injection rate decreases. Recall from §5.2.2 that in the limit of an infinitely thin middle layer, the flow will be stable when Q satisfies (5.16). The injection rate obtained by taking the minimum value of Q over all n from equation (5.16) is also given in Figure 10. Equation (5.16) is the same condition as the stable injection rate for two-layer flow but with effective interfacial tension $T_0 + T_1$. Therefore, a three-layer flow with a very thin intermediate layer will be stable for faster injection rates than the corresponding two-layer flow as long as the sum of the interfacial tensions in the three-layer flow is greater than the interfacial tension of the two-layer flow. Note that this does **not** depend on the viscosity of the intermediate fluid.

Recall that an injection rate that satisfies the condition (5.23) ensures that a flow with N internal layers (or $N+2$ layers) is stable. This bound was computed for flows with four, five, and six layers and plotted in Figure 11. For comparison, the maximum injection rate which results in a stable flow is plotted for two-layer flow (see equation (5.3)) as is the bound for three-layer flow given by equation (5.6). In order to have a fair comparison, each flow is taken to have the same initial position of its outermost interface ($R_N(0) = 10$). For all flows with more than one interface, the innermost interface has an initial position of $R_0(0) = 6$ and the other interfaces are evenly spaced at time $t = 0$. For all flows, the innermost fluid has a viscosity of $\mu_i = 2$, the othermost fluid has a viscosity of $\mu_0 = 10$, and the viscosities of all intermediate layers are chosen so that the viscous jump at each interface is the same. All values of interfacial tension are the same. Note that the three-layer bound given by equation (5.6) allows for the fastest injection rate. That is because the bound is derived using Gershgorin's Circle Theorem and is closer to optimal than the bounds given by equation (5.23). In particular, the bound (5.23) cannot be optimal because the interfaces have been decoupled while Gershgorin maintains the coupling of the interfaces. However, by comparing four, five, and six-layer flows, it can be seen that the addition of more fluid layers increases the injection rate that can be used for a stable flow. This is because the jumps at the interfaces are smaller when there are more layers of fluid.

6.3. *Time-dependent Injection Rate: Stable Manifold*

Finally, we numerically investigate the analytical findings of §5.3 in which it was found that by choosing an appropriate time-dependent injection rate, there will be an eigenvector of the form $\begin{pmatrix} 1 & 0 \end{pmatrix}^T$ for three-layer flows which persists for all time and the span of this eigenvector is a stable manifold. Therefore, if only the inner interface is disturbed initially, the outer interface will remain circular for all time (with no disturbance) and the disturbance of the inner interface will decay. This is seen in Figure 12 by the curve labeled "eigenvector." This curve corresponds to an initial disturbance of $\begin{pmatrix} 0.1 & 0 \end{pmatrix}^T$, which is an eigenvector of the matrix $\mathbf{M}_1$ (see equation (2.12)). As a comparison, the curve labeled "perturbed eigenvector" has an initial disturbance of the form $\begin{pmatrix} 0.1 & 0.0001 \end{pmatrix}^T$. This perturbed eigenvector is just off of the stable manifold. Although the eigenvalue associated with the eigenvector $\begin{pmatrix} 1 & 0 \end{pmatrix}^T$ is negative, the parameters chosen are such that the eigenvalue associated with the other

eigenvector is positive throughout the simulation and therefore the flow is unstable. Therefore, the contribution of the other eigenvector will grow. Notice that for short time the perturbed eigenvector behaves like the eigenvector but then the disturbances of both the inner and outer interfaces begin to grow. Therefore, a very small difference in the initial condition leads to wildly different behavior at later times.

In Figure 13, the interfaces are plotted for both the case in which the initial condition is an eigenvector (Figure 13a) and the case in which it is a perturbed eigenvector (Figure 13b) for three different times. Again, it is difficult to see the differences when the entire interface is plotted so we provide a closer look in Figure 14. At time $t = 0$, the difference between the eigenvector and the perturbed eigenvector is so small that it cannot easily be discerned in the figures (see Figure 14a). However, at later times there is a clear difference (see Figures 14b and 14c). At times $t = 150$ and $t = 300$, the outer interfaces that correspond to an eigenvector disturbance are circular while the inner interfaces are nearly circular. However, there is clearly a disturbance in the case of the perturbed eigenvector and the difference between the two cases become more pronounced from time $t = 150$ to $t = 300$.

These results mean that the proper injection rate can result in a stable manifold which consists of one perfectly circular interface and one interface with a perturbation containing a single wave. If a disturbance is on the stable manifold then the prescribed injection rate would result in the disturbance decaying, even if the configuration (i.e. the set-up consisting of all but one circular interfaces and one perturbed circular interface) itself is unstable to disturbances on the circular interfaces. Therefore, in practice it may be difficult to realize such a flow.

7. Conclusion

In this paper, the linear stability of multi-layer immiscible Hele-Shaw and porous media flows has been investigated. The system of ODEs that governs the evolution of interfacial disturbances for three-layer flows, which has been derived previously, has been extended to flows with an arbitrary number of fluid layers. By studying the matrices and their eigenvalues, several key results about time-dependent injection rates are found which can be used to stabilize the flow. In applications like oil recovery, it can be advantageous to inject fluid as quickly as possible while maintaining a stable flow. For two-layer flows, the maximum injection rate for which a disturbance with a particular wave number is

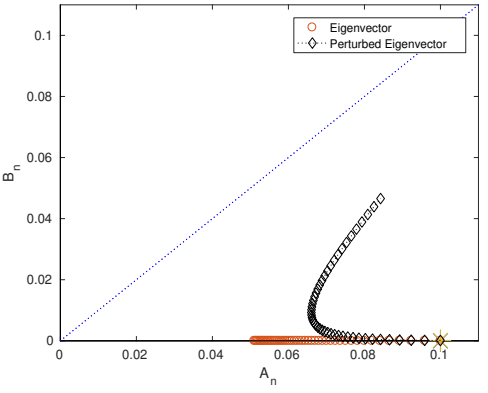

Figure 12: Plots of the amplitude of interfacial disturbances when the injection rate is given by the formula (5.24). The curve labeled "eigenvector" is an eigenvector of $\mathbf{M}$ and the curve labeled "perturbed eigenvector" is given a small perturbation. The parameter values are $Q = 100, \mu_i = 2, \mu_1 = 3, \mu_o = 10, T_0 = 1, T_1 = 0.1, R_0(0) = 28, R_1(0) = 30, n = 20,\ A_{20} = 0.1,\ B_{20} = 0, 0.0001,\ 0 \leqslant t \leqslant 120$. Recall that $A_n(t)$ denotes the amplitude of the disturbance of the inner interface and $B_n(t)$ the outer interface.

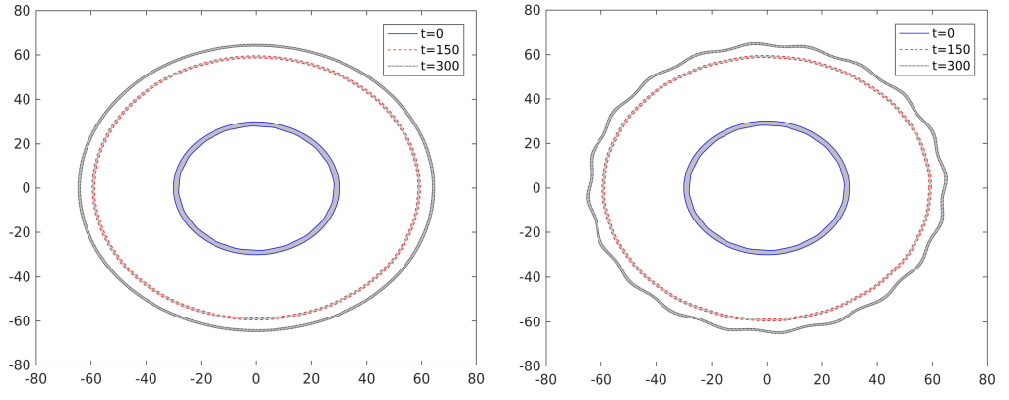

Figure 13: Plots of the interfaces when the injection rate is given by the formula (5.24) (see Figure 12). Plot (a) has an initial disturbance which is an eigenvector of $\mathbf{M}_1$ and (b) has an initial disturbance which is a perturbed eigenvector.

stable is given byBeeson-Jones & Woods (2015). A similar condition is found in the present work for three-layer flows by using Gershgorin's circle theorem. By using upper bounds derived by Gin & Daripa (2015) a sufficient condition on the injection rate to ensure stability is found for a flow with an arbitrary number of fluid layers.

In general the eigenvectors of the matrices $\mathbf{M}_N$ (see equation (4.13)) are time-

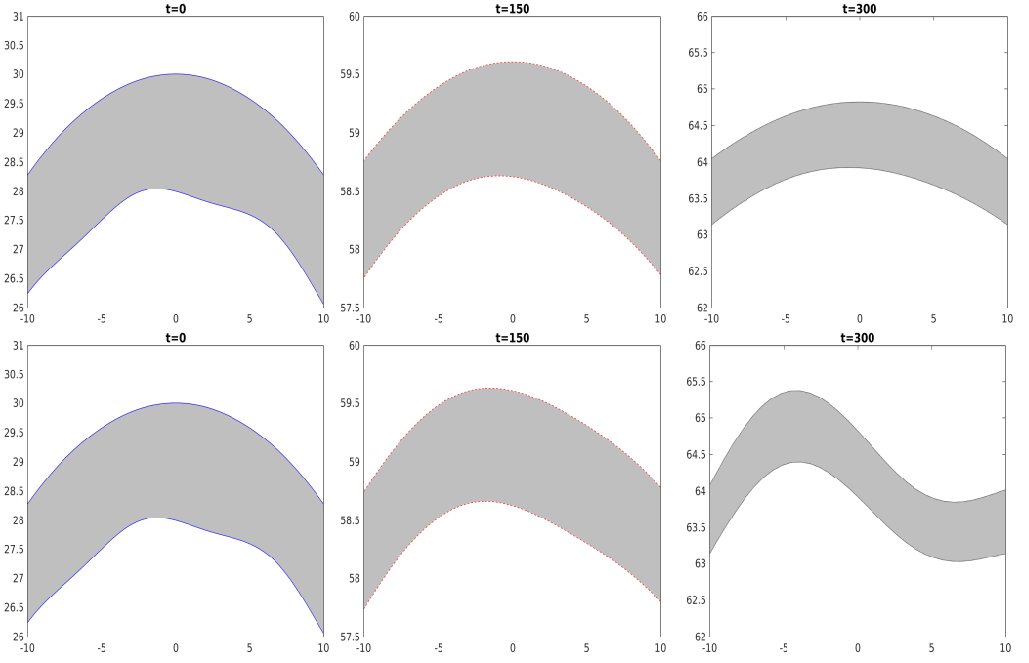

(a) (b) (c)

Figure 14: Plots of the interfaces when the injection rate is given by the formula (5.24) (see Figure 12) at times (a) $t = 0$, (b) $t = 150$, and (c) $t = 300$. The top row shows the interfaces when the initial condition is an eigenvector of $\mathbf{M}_1$ and the bottom row shows the interfaces when the initial condition is a perturbed eigenvector.

dependent. However, with a properly prescribed injection rate, an eigenvector can persist for all time. The eigenvector is such that only one of the interfaces has a disturbance while the other interfaces are circular. The span of the time-independent eigenvector is a stable manifold, and therefore the circular interfaces remain circular for all time while the disturbance on the perturbed interface decays. This result can be achieved regardless of the viscosities of the fluids and the values of interfacial tension as long as the viscosity jump is positive in the direction of flow at each interface.

The behavior of the interfaces and the growth rates of disturbances are investigated numerically and the following results are found: (a) A disturbance which is initially stable can become unstable at later times; (b) The interfaces are coupled so that a disturbance on one interface is transferred to the other interface(s); (c) The disturbances on the interfaces can be in phase or out of phase and there can be a transition from one state to the other; (d) The most dangerous wave number changes with time and

in general there is a cascade to higher modes being more unstable at later times; (e) Flows with more fluid layers can be stable with faster injection rates than comparable flows with fewer fluid layers; and (f) The use of an injection rate that gives a time-independent eigenvector as found in §5.3 results in a flow with all but one circular interfaces and one perturbed circular interface with disturbances on the perturbed circular interface decaying. However, a small perturbation in the eigenvector which corresponds to infinitesimally disturbing one or more of the circular interfaces can disturb all interfaces in time $t = 0^+$ that may grow in amplitude all the while keeping the injection rate same.

Acknowledgments:

This work has been supported in part by the U.S. National Science Foundation grant DMS-1522782.

REFERENCES

Al-Housseiny, T.T. & Stone, H.A. 2013 Controlling viscous fingering in tapered Hele-Shaw cells. *Phys. Fluids* **25** (092102).

Bataille, J. 1968 Stability of a radial immiscible drive. *Revue Inst. Pétrole* **23** (11), 1349–1358.

Beeson-Jones, T.H. & Woods, A.W. 2015 On the selection of viscosity to suppress the Saffman-Taylor instability in a radially spreading annulus. *J. Fluid Mech.* **782**, 127–143.

Cardoso, S.S.S. & Woods, A.W. 1995 The formation of drops through viscous instability. *J. Fluid Mech.* **289**, 351–378.

Coussot, P. 1999 Saffman-Taylor instability in yield-stress fluids. *J. Fluid Mech.* **380**, 363–376.

Darcy, H. 1856 Les Fontaines Publiques de la Ville de Dijon. *Paris* .

Daripa, P. 2008*a* Hydrodynamic stability of multi-layer Hele-Shaw flows. *J. Stat. Mech. Theory Exp.* **12**, 28.

Daripa, P. 2008*b* Studies on Stability in Three-Layer Hele-Shaw flows. *Phys. Fluids* **20** (11).

Daripa, P. & Ding, X. 2012 A numerical study of instability control for the design of an optimal policy of enhanced oil recovery by tertiary dispalcement processes. *Transport in Porous Media* **93(3)**, 673–703.

Daripa, P. & Ding, X. 2013 Selection principle of optimal profiles for immiscible multi-fluid Hele-Shaw flows and stabilization. *Transport in Porous Media* **96** (2), 353–367.

Daripa, P. & Gin, C. 2016 Studies on dispersive stabilization of porous media flows. *Physics of Fluids* **28** (8).

Dias, E.O., Alvarez-Lacalle, E., Carvalho, M.S. & Miranda, J.A. 2012 Minimization of viscous fluid fingering: a variational scheme for optimal flow rates. *Phys. Rev. Lett.* **109**.

Dias, E.O. & Miranda, J.A. 2011 Influence of inertia on viscous fingering patterns: Rectangular and radial flows. *Phys. Rev. E* **83** (6, 2).

Fontana, J.V., Dias, E.O. & Miranda, J.A. 2014 Controlling and minimizing fingering instabilities in non-Newtonian fluids. *Phys. Rev. E* **89**.

Gin, C. & Daripa, P. 2015 Stability results for multi-layer radial Hele-Shaw and porous media flows. *Physics of Fluids* **27** (1).

He, A., Lowengrub, J. & Belmonte, A. 2012 Modeling an elastic fingering instability in a reactive Hele-Shaw flow. *SIAM J. Appl. Math.* **72** (3), 842–856.

Homsy, G.M. 1987 Viscous fingering in porous media. *Annu. Rev. Fluid Mech.* **19**, 271–311.

Li, S., Lowengrub, J., Fontana, J. & Palffy-Muhoray, P. 2009 Control of viscous fingering patterns in a radial Hele-Shaw cell. *Phys. Rev. Lett.* **102** (17).

Paterson, L. 1981 Radial fingering in a Hele-Shaw cell. *Journal of Fluid Mechanics* **113**, 513–529.

Saffman, P.G. & Taylor, G. 1958 The penetration of a fluid into a porous medium or Hele-Shaw cell containing a more viscous liquid. *Proc. R. Soc. Lond. Ser. A* **245**, 312–329.

Wilson, S.D.R. 1975 Measurement of dynamic contact angles. *J. Colloid Interface Sci.* **51** (3), 532–534.

Zheng, Z., Kim, H. & Stone, H.A. 2015 Controlling viscous fingering using time-dependent strategies. *Physical Review Letters* **115** (174501).